Thermal Advances 7 (2026) 100131

Contents lists available at ScienceDirect

Thermal Advances

journal homepage: www.elsevier.com/locate/thradv

Full Length Article

Thermophysical characteristics of tricosane-hexatriacontane blends for phase change material applications

Jana Zimmermann [a,b], Tom Schulz [a], Manisha Kabi [a], Michael Fischlschweiger [c,*]

[a] Clausthal University of Technology, Chair of Technical Thermodynamics and Energy Efficient Material Treatment, Agricolastraße 4, Clausthal-Zellerfeld 38678, Germany
[b] Karlsruhe Institute of Technology, Institute of Technical Thermodynamics and Refrigeration Technology, Engler-Bunte-Ring 21, 76131 Karlsruhe, Germany
[c] Karlsruhe Institute of Technology, Institute of Technical Thermodynamics, Engelbert-Arnold-Str. 4, 76131 Karlsruhe, Germany

ARTICLE INFO

Keywords:
Thermal energy storage
Actuators
Phase change materials
Order-disorder-transition
Order-order transition
Tricosane
Hexatriacontane

ABSTRACT

Phase change materials are crucial for many applications in thermal energy storage and the development of self-adaptive micro actuators. Organic phase change materials, particularly n-alkanes, have been successfully used for these purposes. Key challenges include expanding the range of applications by accessing additional phase transformation zones and their associated phase change energies. Blends of n-alkanes offer a way to tailor thermophysical properties. In this study, the thermophysical properties of the n-alkanes tricosane (C23) and hexatriacontane (C36), as well as their binary mixtures, are investigated over the temperature range of 30 to 80 °C. We observed a melting-point depression of up to 18 K for hexatriacontane and a non-linear change in heat of fusion by up to 6 % over the composition. In particular, the change in melting point of these n-alkane mixtures shows potential to tailor the temperature window of this PCM. This work provides new thermophysical property data on these alkanes and addresses thermal rate effects and mixture data, creating a database to support the future development of latent heat storage systems or micro actuators based on tricosane and hexatriacontane blends.

1. Introduction

Phase change materials (PCMs) are capable of storing substantial amounts of energy. Latent heat thermal energy storage (LHTES) utilizing PCMs is a key method for thermal energy storage (TES) [1,2]. These materials are especially valued for their ability to regulate temperature and store a specific amount of energy over a certain time window. Consequently, PCMs are widely used to help reduce heating and cooling demands. Examples according to Ref [1] include their application in thermal insulation for buildings [1,3], delaying freezing by melting snow/ice on concrete roads [4], food packaging [5], textiles [6], battery technology [7], and cooling photovoltaic panels [8]. In particular, solid-liquid phase change PCMs are popular because they undergo comparably less volume change during phase transition and offer a broad range of phase change temperatures [9–11].

Organic PCMs [12–15], particularly paraffins, are effective due to their appropriate operating temperature ranges, high latent heat, affordability, and principal capability for isothermal operation [16,17]. Paraffins are alkanes with usually linear or branched structures featuring single carbon-carbon bonds [16]. Their physical state at room temperature varies with chain length: gaseous ($1 \leqslant n \leqslant 4$), liquid ($5 \leqslant n \leqslant 17$), or solid ($n > 17$) [16]. These paraffins exhibit a melting range, approximately from 30 °C to 100 °C, within which they transition from solid to liquid. They have a heat of fusion ranging from 200 to 250 J g^{-1} (in some cases even up to 270 J g^{-1} [18]) and a thermal conductivity around 0.2–0.4 W mK^{-1} [16,19]. Unlike most other PCMs, paraffins experience two distinct phase transitions when heated: first from solid to solid, and then from solid to liquid [16]. The initial transition involves a change in the crystalline structure, leading to a volume expansion of 2 %–6 % [16]. Following this, the molecular interactions within the paraffins weaken, allowing the carbon chains to move more freely in the liquid phase, which results in an overall volume expansion of 10 %–20 % [16]. Paraffins are often primarily employed as thermal energy storage solutions across various applications. However, their application in actuators is attracting increasing technological interest. Paraffin actuators are devices that utilize paraffin wax to transform certain forms of energy into mechanical motion [16].

The crystalline structure, and consequently the phase transition

* Corresponding author.
E-mail address: michael.fischlschweiger@kit.edu (M. Fischlschweiger).

https://doi.org/10.1016/j.thradv.2026.100131

Available online 23 March 2026

behavior in terms of thermophysical and mechanical properties, depends on the carbon number.

At low temperatures, odd alkanes (from C_{13} to C_{41}) adopt an orthorhombic structure, while even alkanes are divided into triclinic structures (from C_{14} to C_{26}) and monoclinic structures (from C_{28} to C_{36}) [20]. The structures are categorized into two types for this purpose: ordered phases and disordered phases, which are often called rotator phases. The disordered structures occur at higher temperatures, sometimes just before melting [20,21].

Due to their intricate phase transition behavior and the associated variations in thermophysical properties and morphology changes [22–24], these materials are gaining increased attention in energy storage and actuator applications. Particularly, n-alkane blends emerge as promising candidates, as their composition dependent properties allow precise tailoring of PCM characteristics to suit the respective application. In the context of thermal energy storage, besides using eutectic systems, such PCM blends offer the advantage of extending the operational temperature range for heat absorption and release. This is relevant for heat storage applications that operate within a relatively large temperature window between room temperature and 80 °C. Although numerous studies have examined the melting behavior of binary mixtures of long-chain n-alkanes with similar carbon numbers [23], a systematic investigation of mixtures comprising two n-alkanes with a large carbon-number disparity – specifically, combinations of odd and even-numbered components – remains limited. Therefore, this study aims to examine the thermophysical properties of n-alkane tricosane ($C_{23}H_{48}$) and n-alkane hexatriacontane ($C_{36}H_{74}$), focusing on melting points, crystallization temperatures, and their respective enthalpies with high precision and particularly low thermal rate conditions during property investigation. Tricosane is a common n-alkane in research investigations (e.g. [25]) and as a microencapsulated PCM for electronics, whereas hexatriacontane is more commonly utilized as a higher-melting component in blends, designed for applications such as solar thermal heat storage [26]. The combination of these n-alkanes has not been investigated yet, to the author's knowledge. In the following paragraph, the known phase transition of tricosane (Fig. 1) and hexatriacontane (Fig. 2) are presented [27].

At low temperatures, tricosane exists in an orthorhombic, ordered phase. Around 37.5 °C, the first transformation, called δ-transformation, occurs. The orthorhombic crystal structure remains, but the space groups are now arranged in Pbnm, according to Herrman Maguin's notation [20,21,28,29]. This is followed by the o-d transformation at approximately 39.5 °C, where the ordered phase disappears, leaving only disordered phases. The next transition at a higher temperature results in the first rotator phase, more precisely beta-RI (Fmmm), which also has an orthorhombic structure but is slightly modified due to rotation along the axis. Unlike the previous transformations, this is a second-order phase change. With further heating, the first rotator phase transforms into the second, rhombohedral rotator phase, alpha RII (R3m). Finally, around 47 °C, the melting process occurs, involving the largest phase transformation in terms of energy [20,21,28].

Hexatriacontane exists at low temperatures in an ordered, monoclinic phase (Fig. 2). The monoclinic form transforms into an orthorhombic form at approximately 70.5 °C through a crystal-to-crystal transformation. The order-disorder transformation occurs at around 72 °C, leaving the ordered state and forming the hexagonal rotator phase. The hexagonal phase melts at about 74 °C, turning into liquid. The presence of different phases can be disturbed by impurities, causing phases to disappear at low purity or to appear at different temperatures [30].

In this work, the focus is on producing blends of tricosane and hexatriacontane and, for the first time, experimentally investigating their thermophysical properties and complex phase transformation behavior as a function of composition. The goal is to develop a data basis in terms of thermophysical information for designing new thermal energy storage systems and micro actuators based on PCM blends composed of tricosane and hexatriacontane for future applications.

2. Materials

The n-alkane tricosane ($C_{23}H_{48}$) (purity >99 %) and n-alkane hexatriacontane ($C_{36}H_{74}$) (purity >98 %) were purchased from BLDpharm and used as received. Binary mixtures were prepared gravimetrically (balance accuracy ± 0.01 mg), followed by melting both components at 90 °C and subsequent solidification at room temperature. The sample mass for the DSC measurements was varied between 10 mg and 135 mg as discussed in detail in Section 4.1.

3. Methods

A 3D Calvet calorimeter from Setaram is used to determine the order-disorder enthalpies with high precision. The 3D sensor is constructed such that two cylindrical thermopiles fully surround the sample and reference cell with 144 thermocouples each. Each thermopile enables

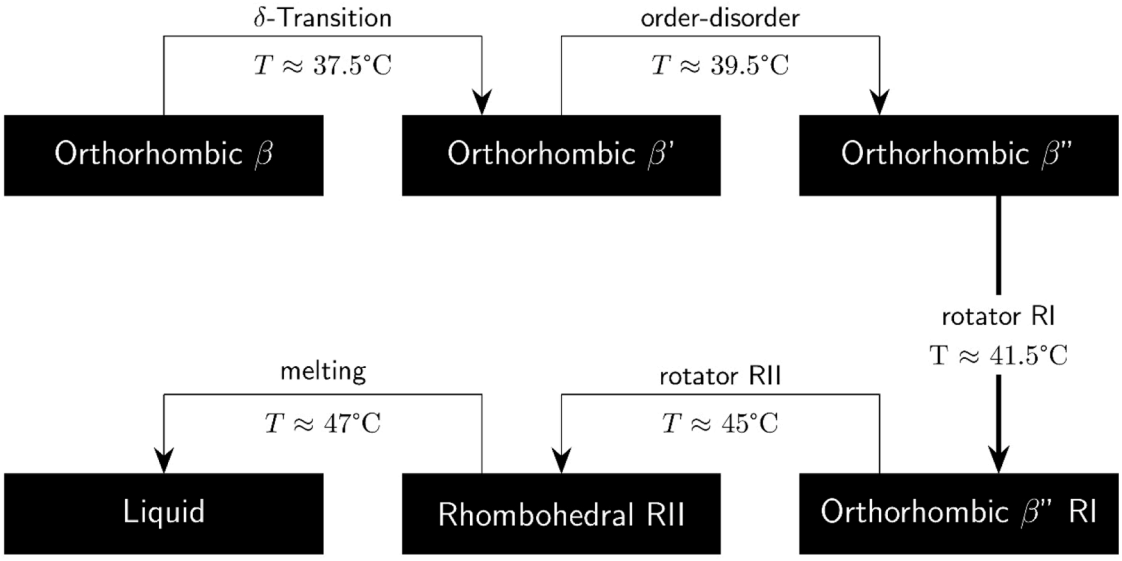

Fig. 1. The phase transformations of tricosane with increasing temperature. Experimental information from Ref [27,28].

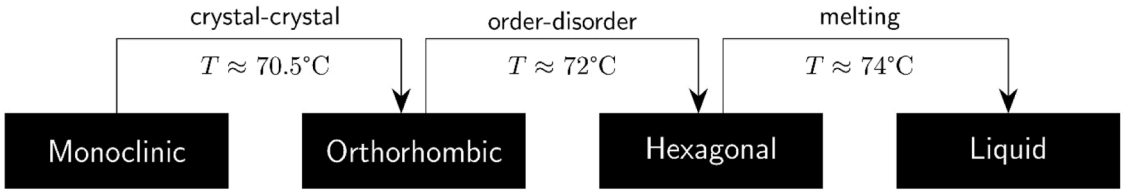

Fig. 2. The phase transformations of hexatriacontane with increasing temperature. Experimental information from Ref [27,30].

the quantitative capture of heat absorbed or released by each cell in all directions. This architecture minimizes lateral heat losses and leads to a high efficiency regarding the heat released or absorbed by the sample (up to 95% according to the manufacturer). The system can be operated between room temperature and 600 °C. To calibrate the temperature, a four-point calibration is performed with high-purity metals (indium, bismuth, zinc, and tin) at heating rates between 0.05 and 1 K min^{-1}. The enthalpy is calibrated using a Joule effect calibration procedure performed by the manufacturer. The measurement uncertainties are ± 1 K for temperature and ± 1 % for enthalpy.

Sample masses between 10 mg and 135 mg are weighed. To homogenize the samples, the alkanes are completely melted at 90 °C and mixed with a glass rod. The cooled sample is then placed in the calorimeter. To investigate order-disorder-transitions, the sample is heated from room temperature to 90 °C and then cooled back to room temperature. The experiments are run at a heating rate of 0.05 K min^{-1} or 0.1 K min^{-1}. Due to the particularly low heating rates, the thermodynamic equilibrium state can be assumed, and significant influences of kinetic effects can be excluded. Furthermore, the heat flow signals are corrected by mass and heating rate to compare the heating rate and sample mass independently. Thus, the normalized enthalpies are available to facilitate a proper comparison. The onset- and offset temperatures are determined by the intersection of the peak tangents and the baseline. To evaluate convoluted peaks, peak deconvolution by Gauss-Lorentz cross is performed. A comparison of the deconvolution by Gauss, Lorentz, and Gauss-Lorentz is available in the appendix.

For the sake of completeness, the Gauss-Lorentz model is presented in eq. (1).

$$\dot{Q}(T) = \frac{\widehat{A}}{1 + \exp\left(\frac{1-s}{2}\left(\frac{T-T_c}{b}\right)^2\right) \cdot s\left(\frac{T-T_c}{b}\right)^2} \tag{1}$$

$\dot{Q}$ is the heat flow, $\widehat{A}$ is the amplitude, T is the temperature, T_c stands for the temperature of the peak maximum, b is the half-width, and s is a shape parameter.

The Gaussian-Lorentzian-model is a hybrid between the Gaussian- and the Lorentzian-model. Therefore, the Gaussian-Lorentzian-model has benefits from both types: The sharp maxima regions are well described by the Gaussian part, and the "wings" can be modeled through the Lorentzian model part, this can also be seen by comparing the total enthalpies in previous literature [31]. The Gaussian-model underestimates the total enthalpy, where the Lorentzian-model overestimates the total enthalpy by nearly 9 %.

4. Results and discussion

This section presents the results for the alkanes tricosane, hexatriacontane, and their binary blends. First, the results for the pure alkanes are shown and compared with data from the literature. Additionally, the hysteresis is examined, and the influence of sample parameters is discussed. Next, the results for the binary blends are presented, which, to the author's knowledge, are investigated at the mixture level for the first time in this work. Here, the effects of alkane interactions on phase change temperatures and enthalpy are established and discussed.

4.1. Tricosane

Fig. 3 shows the DSC measurement of tricosane with the accompanying phase transitions at a heating rate of 0.05 K min^{-1} and a sample mass of 135 mg.

Fig. 3a) shows the o-d transition and melting during heating and the d-o transition and the crystallization of tricosane while cooling, respectively. The hysteresis effect also appears, as heating takes place at a higher temperature than crystallization. For example, the difference in peak temperature between heating and cooling for the solid-liquid transformation is about 2.6 K. The hysteresis also affects the width of the order-disorder transition and melting peak. Notably, the o-d conversion peak is wider during melting than during crystallization. This can be seen in the difference between onset and offset temperatures; it is observed that this difference for the o-d transition during crystallization is smaller (0.5 K) compared to that during melting (1.5 K). On the contrary, the difference between onset and offset temperatures for solid-liquid transition is similar, 2.2 K for melting and 2.1 K for crystallization.

Fig. 3b) presents the enlarged heat flow signal of the phase transitions. Here, four peak transitions are observable, namely the δ-transition, the order-disorder transition (o-d), the rhombohedral II transition (RII), and the melting of tricosane. The rotator I transition is not visible and probably obscured by the much larger o-d-transition.

In Fig. 4, the impact of heating rate is investigated as the heating rate is varied between 0.05 K min^{-1} and 0.1 K min^{-1}.

As shown in Fig. 4, the onset temperatures of both the o-d transition and the melting do not depend significantly on the heating rate in the respective range. However, the offset temperatures as well as the peak maximum temperatures increase with increasing heating rate. The offset temperature of the o-d transition is increased by about 2 K. The peak maximum temperatures increase by around 2 K (o-d transition) and 1 K (melting), respectively.

To investigate size effects, we also examined different sample masses, as shown in Fig. 5. The results of a 135 mg sample and a 20 mg sample are compared with a heating rate of 0.05 K min^{-1} each.

The utilization of a smaller sample mass leads to sharper peaks as thermal lag effects within the sample are reduced. Again, the onset temperatures do not vary greatly with sample mass. Samples with a mass lower than 20 mg resulted in a decrease in signal-to-noise ratio and were therefore not investigated further.

To summarize the findings for tricosane, the measured transformation temperatures are reported in Table 1 and compared to literature values.

A summary of the measured phase change enthalpies is shown in Table 2 and compared to literature values.

The measured values correspond to the data in the literature with no greater deviation than 10%. As presented in Fig. 4, in this work, we applied small heating rates for the investigation of phase transitions which results in a detection of the transition enthalpies where kinetic effects are suppressed.

4.2. Hexatriacontane

The phase transitions of hexatriacontane are analyzed similarly to tricosane by DSC measurements. Firstly, the phase transformations are identified, and the associated hysteresis is examined. For this purpose, a

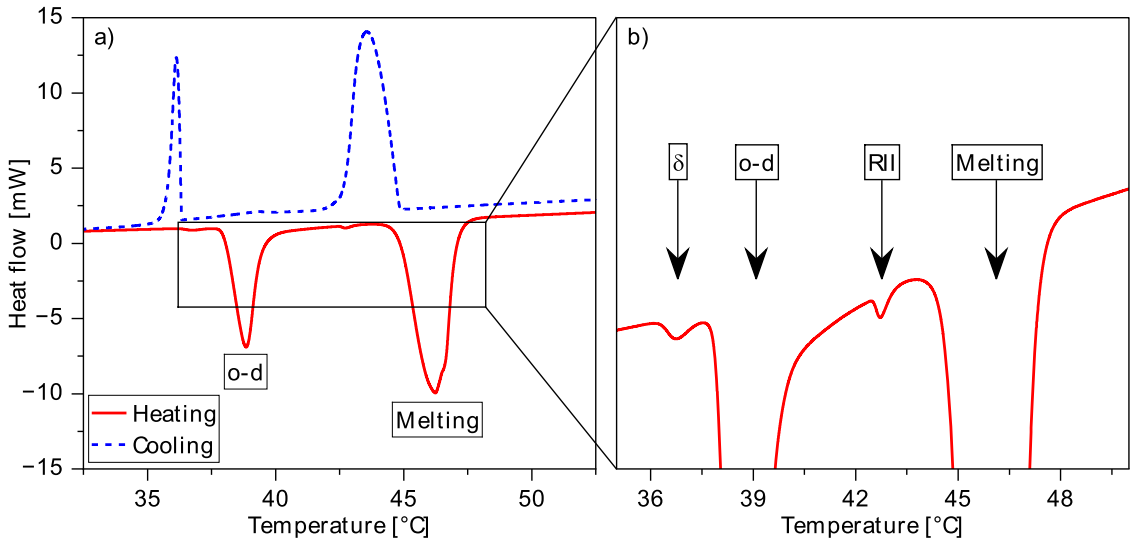

Fig. 3. a) Heat flow of tricosane during heating (red solid line) and cooling (blue dashed line) (mass of 135 mg and heating rate of 0.05 K min^{-1}), b) enlarged heat flow signal with marking of transitions, i.e., δ-transition, order-disorder transition (o-d), rhombohedral II transition (RII), and melting.

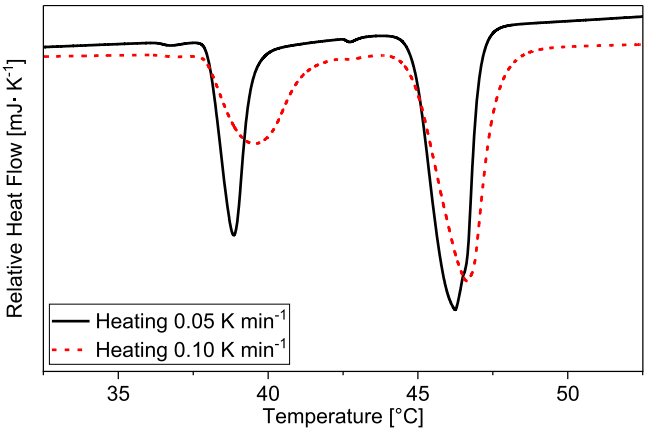

Fig. 4. Effect of the two heating rates on the DSC-signal during heating of tricosane with $\beta_1 = 0.05$ K min^{-1} (black solid line) and $\beta_2 = 0.1$ K min^{-1} (red dashed line).

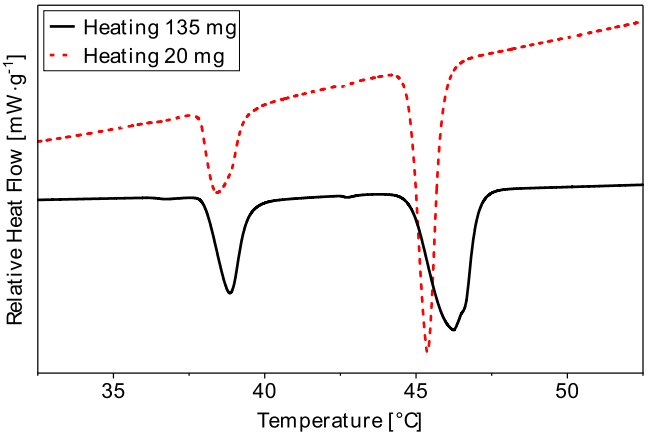

Fig. 5. Effect of the sample mass on the DSC-signal during heating of tricosane with a heating rate of 0.05 K min^{-1}and a mass of 135 mg (black solid line) and 20 mg (red dashed line).

comparison of the melting and crystallization curves of 20 mg

Table 1
Phase transition peak maximum temperatures of tricosane and results reported by the literature [20,21,28,32].

Effect	m	β	T_{fus}	T_{RII}	T_{o-d}	T_{δ}
	[mg]	[K•min^{-1}]	[°C]	[°C]	[°C]	[°C]
Melting	135	0.10	46.7	-	39.5	37.0
		0.05	46.2	42.7	38.9	36.7
	20	0.05	45.4	42.7	38.4	-
Dirand et al. [20]	unk.	unk.	47.25	-	42.45	-
Chevallier et al. [21]	unk.	0.5	47.76	45.50	40.70	38.00
Robles et al. [28]	unk.	unk.	47.15	44.75	39.25	37.35
Crystallization	135	0.10	43.6	-	36.5	-
		0.05	43.6	-	36.1	-
	20	0.05	44.5	42.4	36.3	-
Hammami et al. [32]	4–8	1–10	46.5	-	38.6	-

*Standard uncertainties of this work for T_i were 1 K.

Table 2
Overview of the measured enthalpies of the phase transitions for tricosane compared to literature values [20,21,28].

Effect	m	β	ΔH_{fus}	ΔH_{RII}	ΔH_{o-d}	ΔH_{tot}
	[mg]	[K•min^{-1}]	[J•g^{-1}]	[J•g^{-1}]	[J•g^{-1}]	[J•g^{-1}]
Melting	135	0.10	152.5	-	67.1	219.6
		0.05	153.8	0.5	69.6	223.9
	20	0.05	150.4	0.4	65.2	216.0
Dirand et al. [20]	unk.	unk.	163.7	-	66.9	230.6
Chevallier et al. [21]	unk.	0.5	156.7	-	71.	227.7
Robles et al. [28]	unk.	unk.	162.0	0.99	60.4	223.4
Crystallization	135	0.10	156.3	-	54.9	211.2
		0.05	157.4	-	54.2	211.6
	20	0.05	150.4	0.6	52.4	203.4

* Standard uncertainties of this work were 1 % for ΔH_i.

hexatriacontane at a heating rate of 0.05 K•min^{-1} was investigated and is presented in Fig. 6.

Hexatriacontane shows three peaks in the DSC curves that are closer together compared to tricosane (Fig. 3). As a result, the peaks partially overlap, making the analysis more complicated. Despite the overlap, each peak can still be assigned to the phase transitions described in Fig. 2.

In Fig. 6 for the heating path, the first peak corresponds to the

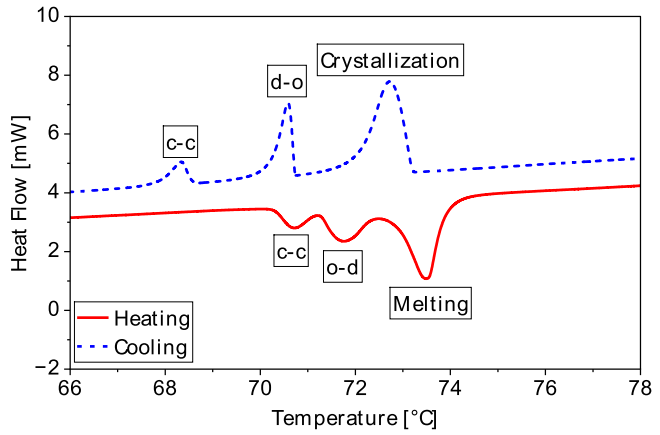

Fig. 6. Heating (red solid line) and cooling (blue dashed line) of hexatriacontane with a mass of 20 mg and heating rate of 0.05 K·min^{-1} with marking of transitions, i.e., crystal-crystal transition (c-c), order-disorder transition (o-d), and melting.

crystal-crystal transformation (c-c). The second peak relates to the o-d transformation (o-d). The final peak, indicating the melting process, shows the highest phase transformation enthalpy.

The on-set and off-set temperatures, as well as the peak shape, are different for heating and cooling cycles. The peak separation is more pronounced during crystallization than during melting. This is because of the greater supercooling of solid-solid transitions compared to solid-liquid phase transitions. The supercooling increases the distance between peaks, enhancing their separation. The crystal-crystal transition exhibits significantly greater supercooling, with a value of 2.4 K compared to 1.2 K for the solid-liquid transition, indicating a thermal hysteresis effect. The melting process is closer to thermodynamic equilibrium, and crystallization is more kinetically controlled. Kinetic effects due to heat transfer are negligible as low heating rates are applied. During crystallization, nucleation and subsequent growth must first occur. The energy barrier of nucleation causes supercooling and is followed by crystal growth, which often proceeds rapidly. The peak shapes differ between the melting and crystallization processes due to the lamella shapes and thicknesses that form. During crystallization, narrower lamellae form, resulting in an asymmetrical peak shape.

Due to lower diffusion in the solid phase, further supercooling occurs during the o-d transformation and the c-c transformation, which is why the solid-solid-peaks favor peak separation.

The impact of mass on the DSC signal is illustrated in Fig. 7.

Increasing the sample mass improves the signal-to-noise ratio, on the one hand. On the other hand, it causes peaks to convolve and blur into a single, asymmetrical peak with multiple maxima. This effect is lessened by crystallization and the previously mentioned hysteresis. Reducing the sample mass to 10 mg slightly enhances deconvolution compared to a 20 mg sample.

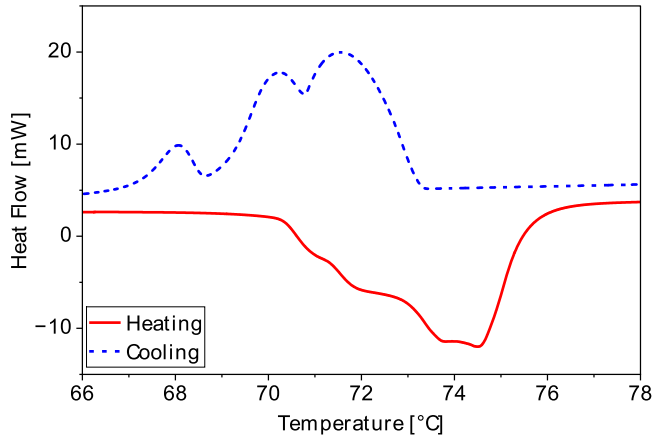

Fig. 7. DSC-curves hexatriacontane during heating (red solid line) and cooling (blue dashed line) with a mass of 120 mg and a heating rate of 0.1 K·min^{-1}.

To fractionate the peaks completely, and thereby gain access to the enthalpy of each phase transition, peak deconvolution by Gauss-Lorentz is applied according to Eq. (1). A comparison with Gauss and Lorentz is available in the appendix. Fig. 8 shows the peak deconvolution by Gauss-Lorentz for hexatriacontane with a mass of 20 mg and a heating rate of 0.1 K·min^{-1}.

In Table 3, the peak maximum temperatures of each transition are given and associated with the respective thermal rate and further compared to literature values.

In Table 4, the phase transformation enthalpies are summarized and compared to literature values. The enthalpies obtained through peak separation using the Gauss-Lorentz function are shown in blue, while the evaluation of the convoluted peaks is shown in black.

The total enthalpy measured in this study aligns well with literature values. The enthalpies for the o-d transformation are relatively high, whereas the melting values are lower than those reported in the literature, which could be associated with certain thermal rates. The next section discusses the phase transitions of the binary blends.

4.3. Binary blends

Four binary blends of tricosane and hexatriacontane are prepared at the lab scale, and all measurements are performed using sample masses of 100 mg with heating and cooling rates of 0.1 K per minute.

In Fig. 9, the four analyzed heat flow curves of the melting mixtures are presented and compared with the information of the pure materials.

Primarily, three peaks are observed for the mixtures: the first two at lower temperatures, shown on the first half of the diagram in terms of temperature, attributable to tricosane, and one at a higher temperature corresponding to hexatriacontane. For the mixture, the shape of the peak for hexatriacontane is significantly broader than that of the pure material, and it increases as the concentration decreases. Additionally, the conversion begins at lower temperatures. The peak maximum temperature of tricosane also decreases with decreasing concentration, but the effect is less pronounced compared to hexatriacontane.

In Fig. 10, the DSC curves of the blends during crystallization are presented.

During cooling, the phase transitions of the blend are better separated and less influenced by the mixing compared to those during

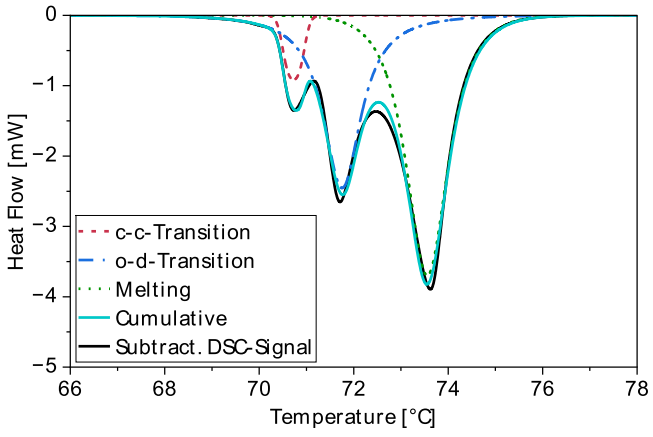

Fig. 8. DSC-signal for peak separation using the Gaussian-Lorentzian function for hexatriacontane with a mass of 20 mg and a heating rate of 0.1 K·min^{-1} with the subtracted DSC-signal (black solid line), crystal-to-crystal transition (red dashed line), the o-d transition (blue dash dotted line), the melting (green dotted line), and the cumulative peak (turquoise solid line).

Table 3
Overview of the measured temperatures of the phase transitions for hexatriacontane with associated thermal rates compared to literature values [18,20,30,33–43].

Effect	m	β	T_{fus}	T_{o-d}	T_{c-c}
	[mg]	[K•min^{-1}]	[°C]	[°C]	[°C]
Melting	130	0.1	74.5	-	-
	20	0.1	73.6	71.7	70.7
		0.05	73.5	71.8	70.7
	10	0.1	73.4	71.5	70.6
		0.05	73.4	71.6	70.6
Crystallization	130	0.1	71.6	70.2	68.1
	20	0.1	72.6	70.6	68.2
		0.05	72.7	70.6	68.3
	10	0.1	72.9	71.0	68.3
		0.05	73.0	71.0	68.3
Dirand et al. [20]	unk.	unk.	75.8	73.6	-
NIST [33–43]	unk.	unk.	76.0 ± 0.9	-	-
Earnest et al. [30]	(1–1.6)	2	74.0	71.9	70.8
Stewart et al. [18]	unk.	0.5	(74.8–74.9)	(72.6–72.7)	(69.9–71.6)

* Standard uncertainties of this work were 1 K for T_i.

Table 4
Overview of the obtained enthalpies of the phase transitions allocated to certain thermal rates for hexatriacontane and compared to literature values [18,20,30][a].

Effect	m	β	ΔH_{fus}	ΔH_{o-d}	ΔH_{c-c}	ΔH_{tot}
	[mg]	[K•min^{-1}]	[J•g^{-1}]	[J•g^{-1}]	[J•g^{-1}]	[J•g^{-1}]
Melting	130	0.1				269.1
			126.4	120.1	19.5	266.0
	20	0.1				245.3
			136.1	94.6	12.8	243.3
		0.05				238.7
			121.3	100.5	16.3	238.1
	10	0.1				247.1
			147.0	85.1	13.9	246.0
		0.05				254.8
			142.1	82.5	30.0	254.6
Crystallization	130	0.1				257.5
			127.6	88.2	35.8	251.6
	20	0.1				254.8
			132.8	85.3	32.4	250.5
		0.05				245.3
			138.0	69.5	28.2	235.7
	10	0.1				248.9
			127.1	91.4	27.7	246.2
		0.05				251.6
			135.7	70.8	27.8	234.2
Dirand et al. [20]	unk.	unk.	172.9	61.3	-	234.2
Earnest et al. [30]	(1–1.6)	2	166.5	57.1	19.6	243.1
Stewart et al. [18]	unk.	0.5	not measured	250.2 269.5 270.4		

* Standard uncertainties of this work were 1 % for ΔH_i.
[a] Values in black are obtained by the whole peak, values in blue are derived from the curve fit with the Gauss-Lorentz model.

heating. In the 80 mol % hexatriacontane blend, two overlapping phase transformations take place. As concentration drops, these phase transitions become indistinguishable from each other. When cooling, rapid nucleation and growth in the hexatriacontane-rich domains quickly increase the heat-release rate to a maximum, then it slowly decreases over a broader temperature range as ordering persists in more stable regions. During heating, a similarly broad transformation occurs due to melting across a range of lamellar thicknesses. Tricosane experiences comparable transformations during both heating and cooling. However, the transformation rate usually peaks earlier during solidification because supercooling reduces the nucleation barrier and speeds up growth.

Determining the enthalpy for hexatriacontane-dominated transitions is complicated by an asymmetric heat capacity baseline: the slope before

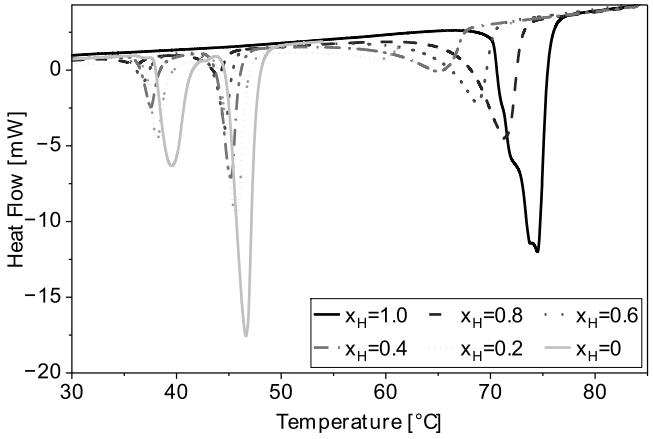

Fig. 9. Heat flow for the heating of the mixtures (100 mg, 0.1 K·min^{-1}, grey lines) and the pure substances tricosane (135 mg, 0.1 K·min^{-1}, light grey solid line) and hexatriacontane (120 mg, 0.1 K·min^{-1} black solid line).

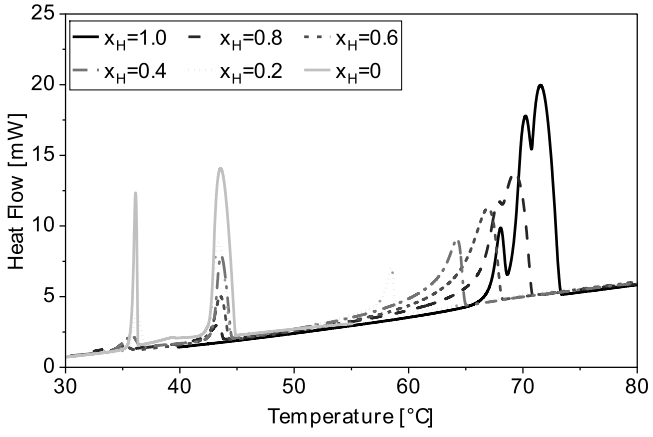

Fig. 10. DSC-curves for the cooling of the mixtures (100 mg, 0.1 K·min^{-1}, grey lines) and the pure substances tricosane (135 mg, 0.1 K·min^{-1}, light grey solid line) and hexatriacontane (120 mg, 0.1 K·min^{-1} black solid line).

the transition differs from the slope after it. This is due to overlapping transformations and broad heat capacity changes that delay the baseline's return to its original level. To evaluate this, a linear baseline anchored after the transition—where the heat capacity has clearly stabilized—is used to ensure consistency with the melting analysis. The hysteresis between melting and crystallization ranges from 1 K for the

blend with 40 mol % hexatriacontane to 4 K for the blend with 10 mol % hexatriacontane. In contrast to the nearly constant phase transition temperatures of tricosane, the phase transition temperatures of hexatriacontane increase as its composition increases. Fig. 11 and Fig. 12 show these temperatures plotted against composition.

In the mixture, the tricosane peak shifts by no more than approximately 2 K during melting and about 3 K during crystallization, while the hexatriacontane peak shifts by over 17 K during melting and roughly 18 K during crystallization. Throughout the mixing series, the temperature of the o-d transformation of tricosane remains nearly constant. Therefore, there is no clear linear relationship between composition and transformation temperature. Additionally, as the hexatriacontane fraction decreases, its peak broadens, suggesting that the phase transition occurs over a wider temperature range rather than sharply at a single point. Other binary, long-chain n-alkane blends, such as $C_{32}H_{66}$+$C_{34}H_{74}$ or $C_{36}H_{74}$+$C_{40}H_{82}$ show no significant shift in melting temperature [23, 25]. When alkanes with similar chain length are blended (e.g. $\Delta n < 4$), the influence of the mixture on the melting temperature is low. In the case of alkane blends with a large difference in chain length, as in this work ($\Delta n = 13$), the influence is greater and can be used to adjust the melting temperature by varying the mixing ratio.

The results indicate that tricosane interferes with the crystallization of hexatriacontane. During cooling, the hexatriacontane-rich regions crystallize first and incorporate dissolved tricosane molecules. This leads to a decrease in the melting temperature and a broadening of the melting range upon reheating, suggesting a reduction in lamellar thickness compared to the pure substance. In contrast, the dissolution of hexatriacontane in tricosane lamella appears to be less favorable, as the melting temperature of the tricosane shifts only slightly (about 2 K). These findings highlight that alkane mixtures with even-odd parity are particularly attractive for TES as they enable individual tuning of transition temperatures.

The corresponding enthalpies are compared with theoretical enthalpies predicted under ideal assumptions from the composition-weighted sum of the pure component enthalpies in Fig. 13 and Fig. 14.

With a few exceptions, the enthalpy of the mixture increases with increasing hexatriacontane content. The enthalpy of the mixture as a function of composition deviates slightly from the values predicted under ideal-conditions. The contribution of hexatriacontane follows the ideal trend more closely, whereas tricosane yields lower values. Consequently, the overall enthalpy of the mixture remains slightly below the ideal prediction. A similar behavior has been reported for n-alkane blends with a chain length difference of $\Delta n = 2$, (e. g. $C_{32}H_{66}$+$C_{34}H_{74}$), where a decrease in the heat of fusion of approximately 7–11 % is observed [25]. In contrast, n-alkane blends with $\Delta n = 4$ (e.g. $C_{36}H_{74}$+$C_{40}H_{82}$) exhibit an increase in heat of fusion of about 5–30 % [25].

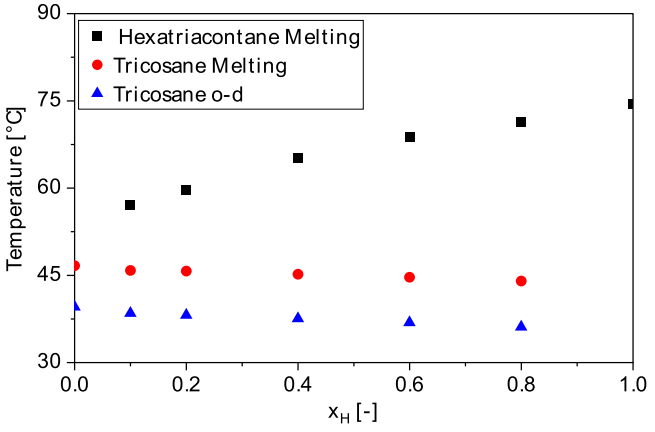

Fig. 11. Peak maximum temperatures of the phase transitions of hexatriacontane (black squares), melting of tricosane (red circles), and o-d transition of tricosane (blue triangles) during heating of the mixtures, depending on their concentration, with a sample mass of 100 mg and a heating rate of 0.1 K·min^{-1}.

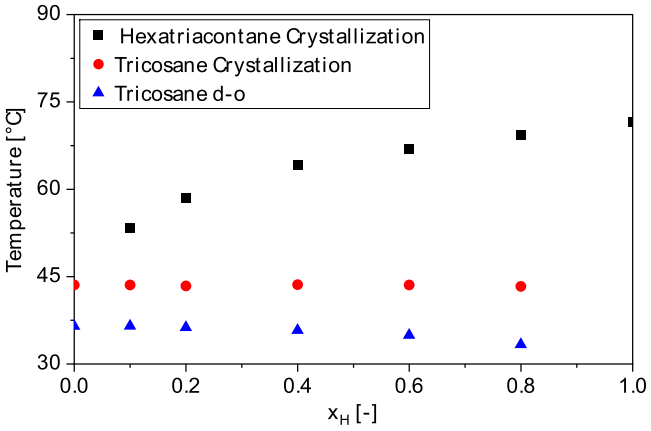

Fig. 12. Peak maximum temperatures of the phase transitions of hexatriacontane (black squares), melting of tricosane (red circles), and D-o transition of tricosane (blue triangles) during cooling of the mixtures, depending on their concentration, with a sample mass of 100 mg and a heating rate of 0.1 K·min^{-1}.

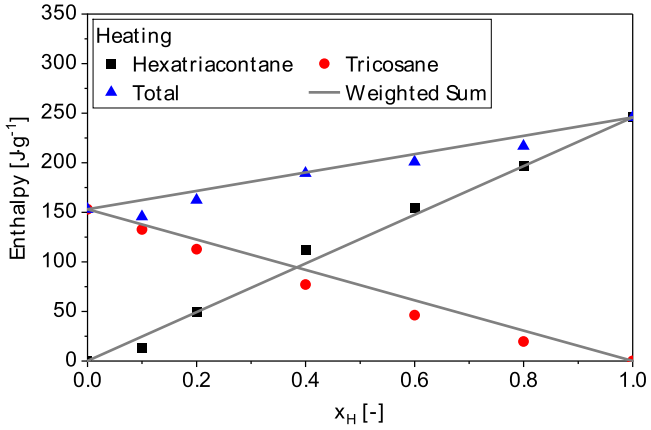

Fig. 13. Enthalpies of the phase transitions of hexatriacontane (black squares), the melting and o-d transition of tricosane (red circles) and the total enthalpy change of the mixture (blue triangles) during heating plotted versus composition, for a sample mass of 100 mg and a heating rate of 0.1 K·min^{-1}, compared with the ideal composition-weighted sum of the pure component enthalpies (grey solid line).

For example, the melting temperature of hexatriacontane decreases by >10 K for a mixture of 20 mol % hexatriacontane (Fig. 11), whereas the melting enthalpy of hexatriacontane remains approximately constant. For tricosane, the melting temperature remains approximately constant, but the enthalpy decreases by about 10 % (Fig. 13).

These findings indicate that small amounts of tricosane are dissolved in the hexatriacontane solid, acting as defects and thereby reducing the melting temperature. The dissolved tricosane molecules persist as a supercooled liquid phase due to their confinement in the hexatriacontane morphology, leading to a reduction in the melting enthalpy of the tricosane component. As the enthalpy of hexatriacontane remains constant, the majority of hexatriacontane transitions into the solid phase, despite the dissolution of tricosane into the phase.

The enthalpy of the mixture increases non-linearly with the proportion of hexatriacontane. When evaluated in comparison to the ideal enthalpy of the mixture, the observed values exhibited a marginal decrease, with a maximum reduction of 6 %, yet remained higher than the melting enthalpy of pure tricosane. The findings indicate that these

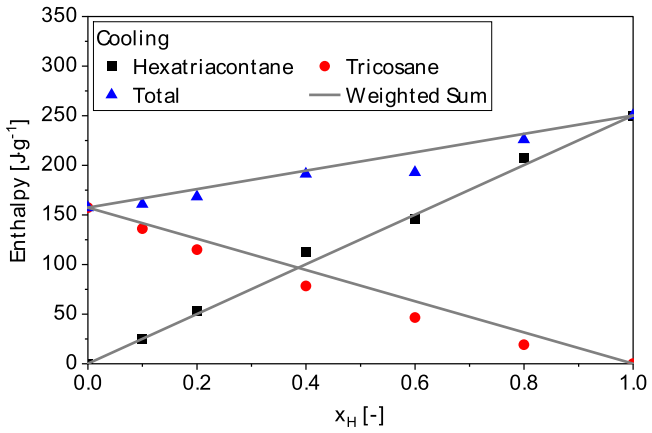

Fig. 14. Enthalpies of the phase transitions of hexatriacontane (black squares), the crystallization and d-o transition of tricosane (red circles) and the total enthalpy change of the mixture (blue triangles) during cooling plotted versus composition, for a sample mass of 100 mg and a heating rate of 0.1 K·min^{-1}, compared with the ideal composition-weighted sum of the pure component enthalpies (grey solid line).

binary alkane blends with notably different chain lengths are promising for heat storage applications in terms of controlling the phase change zone over a larger temperature window. Adding a small amount of tricosane reduces the phase transition temperature of hexatriacontane, allowing for some temperature adjustment. Although this change slightly decreases the enthalpy and broadens the phase transition range, the relationship between enthalpy and composition ensures that the loss in phase transition enthalpy remains minimal at low tricosane concentrations.

5. Conclusions

In this work, the phase transition behavior of the binary mixture of hexatriacontane and tricosane was analyzed using DSC. To this end, the pure substances were first examined, and the influence of heating rate and sample mass was investigated under defined thermal conditions. The phase transition temperatures and enthalpies of the pure components agree well with literature values. In hexatriacontane-rich mixtures, two overlapping thermally driven transformations are observed. On cooling, crystallization proceeds faster within a narrower temperature interval than melting on heating, which occurs over a broader range; this indicates a broader distribution of lamellar thicknesses. Tricosane shows analogous behavior, but its transition temperatures are less sensitive to composition. By contrast, the hexatriacontane transition temperature depends strongly on composition, and no linear relationship is evident. Despite pronounced composition-dependent temperature shifts, the measured enthalpies deviate slightly from the composition-weighted ideal, and the total enthalpy is slightly lower than predicted. In summary, mixtures of alkanes with significantly different chain lengths show promise as heat storage materials: small additions of tricosane lower the transition temperature of hexatriacontane and thereby enable fine temperature tuning of PMCs while incurring only comparably small enthalpy losses. Therefore, this work highlights the importance of alkane mixtures in the context of phase change materials and provides a database for further development of thermal energy storage systems or micro actuators.

CRediT authorship contribution statement

Jana Zimmermann: Writing – original draft, Visualization, Validation, Supervision, Project administration, Methodology, Investigation, Formal analysis, Data curation, Conceptualization. **Tom Schulz:** Writing – original draft, Validation, Methodology, Investigation, Formal analysis, Data curation. **Manisha Kabi:** Writing – original draft. **Michael Fischlschweiger:** Writing – review & editing, Writing – original draft, Supervision, Resources, Project administration, Funding acquisition, Conceptualization.

Declaration of competing interest

The authors declare that they have no known competing financial interests or personal relationships that could have appeared to influence the work reported in this paper.

Acknowledgments

Funded by the Deutsche Forschungsgemeinschaft (DFG, German Research Foundation) 453715850 and by zukunft.niedersachsen, the joint science funding program of the Lower Saxony Ministry of Science and Culture and the Volkswagen Foundation.

Appendix

Fig. A1, A2, Table A1

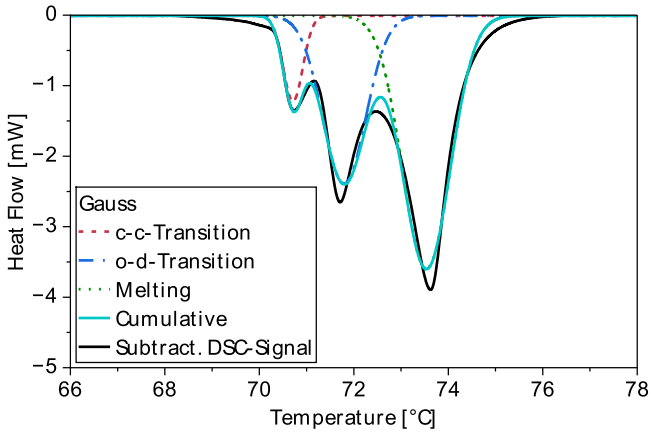

Fig. A1. DSC-signal for peak deconvolution using the Gaussian function with the parameters hexatriacontane with a mass of 20 mg and a heating rate of 0.1 K·min^{-1}. Subtracted DSC-signal (black line), first peak/crystal-to-crystal transition (red dashed line), second peak/o-d transition (blue dashed-dotted line), third peak/melting (green dotted line), cumulative peak (turquoise line).

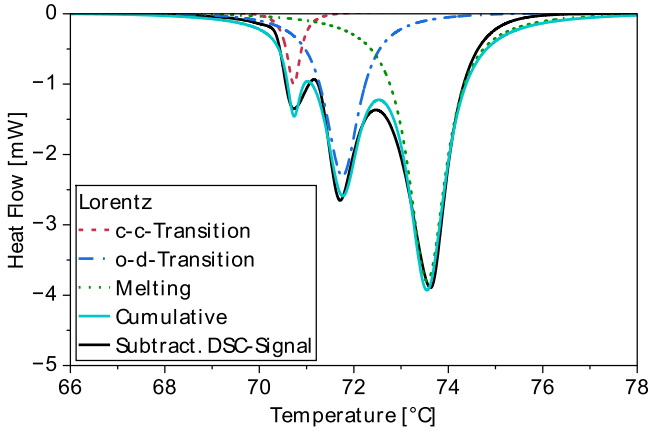

Fig. A2. DSC-signal for peak deconvolution using the Lorentz function with the parameters hexatriacontane with a mass of 20 mg and a heating rate of 0.1 K·min^{-1}. Subtracted DSC-signal (black line), first peak/crystal-to-crystal transition (red dashed line), second peak/o-d transition (blue dashed-dotted line), third peak/melting (green dotted line), cumulative peak (turquoise line).

Table A1
Summary of the enthalpies from the peak separation for hexatriacontane with a mass of 20 mg and a heating rate of 0.1 K·min^{-1}. The enthalpies from the peak separation are listed for the Gauss function (G), Lorentz function (L), and Gauss-Lorentz function (GL).

	m	β	Model	ΔH_{fus}	$\Delta H_{o\text{-}d}$	ΔH_1	ΔH_{tot}
	[mg]	[K•min^{-1}]		[J•g^{-1}]	[J•g^{-1}]	[J•g^{-1}]	[J•g^{-1}]
Melting	20	0.1	-				245.3
			G	134.7	80.5	18.8	234.1
			L	162.4	88.7	15.6	266.8
			GL	136.1	94.4	12.8	243.3

Data availability

Data will be made available on request.

References

[1] C. Alkan, E.H. Alakara, Property development in n-alkane and n-alkane eutectic phase change materials for thermal energy storage applications, Sol. Energy Adv. 5 (2025) 100089, https://doi.org/10.1016/j.seja.2025.100089.

[2] Y.B. Tao, Y.-L. He, A review of phase change material and performance enhancement method for latent heat storage system, Renew. Sustain. Energy Rev. 93 (2018) 245–259, https://doi.org/10.1016/j.rser.2018.05.028.

[3] V.Z. Vargas, L.J. Claros-Marfil, G.F.B. Sandoval, B.H. Rojas, A.G. Santos, Fco.J. N. González, Experimental assessment of energy storage in microencapsulated paraffin PCM Cement mortars, Case Stud. Constr. Mater. 20 (2024) e02959, https://doi.org/10.1016/j.cscm.2024.e02959.

[4] Y. Farnam, H.S. Esmaeeli, P.D. Zavattieri, J. Haddock, J. Weiss, Incorporating phase change materials in concrete pavement to melt snow and ice, Cem. Concr. Compos. 84 (2017) 134–145, https://doi.org/10.1016/j.cemconcomp.2017.09.002.

[5] S. Parvate, J. Singh, J. Reddy Vennapusa, P. Dixit, S. Chattopadhyay, Copper nanoparticles interlocked phase-change microcapsules for thermal buffering in packaging application, J. Ind. Eng. Chem. 102 (2021) 69–85, https://doi.org/10.1016/j.jiec.2021.06.029.

[6] S. Alay Aksoy, C. Alkan, M.S. Tözüm, S. Demirbağ, R. Altun Anayurt, Y. Ulcay, Preparation and textile application of poly(methyl methacrylate-co-methacrylic acid)/n-octadecane and n-eicosane microcapsules, J. Text. Inst. 108 (1) (2017) 30–41, https://doi.org/10.1080/00405000.2015.1133128.

[7] F. Chen, et al., Air and PCM cooling for battery thermal management considering battery cycle life, Appl. Therm. Eng. 173 (2020) 115154, https://doi.org/10.1016/j.applthermaleng.2020.115154.

[8] C. Prieto, L.F. Cabeza, Thermal energy storage (TES) with phase change materials (PCM) in solar power plants (CSP). Concept and plant performance, Appl. Energy 254 (2019) 113646, https://doi.org/10.1016/j.apenergy.2019.113646.

[9] M. Singer, M. Fischlschweiger, T. Zeiner, Investigation of the heat storage capacity and storage dynamics of a novel polymeric macro-encapsulated core-shell particle using a paraffinic core, Energies 16 (2) (2023) 2, https://doi.org/10.3390/en16020957. Art. no.

[10] W. Su, J. Darkwa, G. Kokogiannakis, Review of solid–liquid phase change materials and their encapsulation technologies, Renew. Sustain. Energy Rev. 48 (2015) 373–391, https://doi.org/10.1016/j.rser.2015.04.044.

[11] M. Fischlschweiger, S. Enders, Solid–liquid phase equilibria of binary hydrocarbon mixtures predicted by Lattice cluster theory, J. Mol. Liq. 212 (2015) 436–443, https://doi.org/10.1016/j.molliq.2015.10.005.

[12] L. Geng, J. Cui, C. Zhang, Y. Yan, J. Zhao, C. Liu, Chemistry in phase change energy storage: properties regulation on organic phase change materials by covalent bond modification, Chem. Eng. J. 495 (2024) 153359, https://doi.org/10.1016/j.cej.2024.153359.

[13] L. Geng, T. Xiao, J. Jiang, K. Luo, Y. Yan, C. Liu, Wide temperature range phase change cold energy storage by using esterification between polyethylene glycol and lauric acid, Chem. Eng. J. 496 (2024) 154005, https://doi.org/10.1016/j.cej.2024.154005.

[14] L. Geng, T. Xiao, Y. Cao, G. Li, G. Liang, C. Liu, Chinese tofu-inspired nanocuring: rapid UV-assembled phase change composites with mechanical-thermal synergy, Chem. Eng. J. 523 (2025) 168321, https://doi.org/10.1016/j.cej.2025.168321.

[15] L. Geng, et al., Facile ester-based phase change materials synthesis for enhanced energy storage toward battery thermal management, Adv. Sci. 12 (9) (2025) 2413703, https://doi.org/10.1002/advs.202413703.

[16] S. Morese, P. Woias, U. Pelz, Recent advances in paraffin-based actuation: a pathway to multifunctional systems, Smart Mater. Struct. 34 (8) (2025) 083001, https://doi.org/10.1088/1361-665X/adfb15.

[17] F.L. Rashid, et al., Heat transfer enhancement of phase change materials using letters-shaped fins: a review, Int. Commun. Heat Mass Transf. 159 (2024) 108096, https://doi.org/10.1016/j.icheatmasstransfer.2024.108096.

[18] M.J. Stewart, W.L. Jarrett, L.J. Mathias, R.G. Alamo, L. Mandelkern, Thermally induced molecular motion and premelting in the solid State of *n* -hexatriacontane, Macromolecules 29 (14) (1996) 4963–4968, https://doi.org/10.1021/ma950107k.

[19] H. Mehling, L.F. Cabeza, Heat and cold storage with PCM: an up-to-date introduction into basics and applications. Heat and Mass Transfer, Springer, Berlin, Heidelberg, 2008, https://doi.org/10.1007/978-3-540-68557-9.

[20] M. Dirand, M. Bouroukba, A.-J. Briard, V. Chevallier, D. Petitjean, J.-P. Corriou, Temperatures and enthalpies of (solid + solid) and (solid + liquid) transitions of n-alkanes, J. Chem. Thermodyn. 34 (8) (2002) 1255–1277, https://doi.org/10.1006/jcht.2002.0978.

[21] V. Chevallier, M. Bouroukba, D. Petitjean, D. Barth, P. Dupuis, M. Dirand, Temperatures and enthalpies of solid–solid and melting transitions of the odd-numbered *n*-alkanes C_{21}, C_{23}, C_{25}, C_{27}, and C_{29}, J. Chem. Eng. Data 46 (5) (2001) 1114–1122, https://doi.org/10.1021/je0003501.
[22] C. Liu, P. Du, B. Fang, Z. Li, B. Chen, Z. Rao, Experimental study on a functional microencapsulated phase change material for thermal management, Int. Commun. Heat Mass Transf. 118 (2020) 104876, https://doi.org/10.1016/j.icheatmasstransfer.2020.104876.
[23] S.N. Gunasekara, V. Martin, J.N. Chiu, Phase equilibrium in the design of phase change materials for thermal energy storage: state-of-the-art, Renew. Sustain. Energy Rev. 73 (2017) 558–581, https://doi.org/10.1016/j.rser.2017.01.108.
[24] D. Fu, Y. Liu, X. Gao, Y. Su, G. Liu, D. Wang, Binary n-alkane mixtures from total miscibility to phase separation in microcapsules: enrichment of shorter component in surface freezing and enhanced stability of rotator phases, J. Phys. Chem. B 116 (10) (2012) 3099–3105, https://doi.org/10.1021/jp2125119.
[25] L. Ventolà, et al., Molecular alloys as phase change materials (MAPCM) for energy storage and thermal protection at temperatures from 70 to 85 °C, J. Phys. Chem. Solids 66 (10) (2005) 1668–1674, https://doi.org/10.1016/j.jpcs.2005.06.001.
[26] V.V. Tyagi, et al., A comprehensive review on phase change materials for heat storage applications: development, characterization, thermal and chemical stability, Sol. Energy Mater. Sol. Cells 234 (2022) 111392, https://doi.org/10.1016/j.solmat.2021.111392.
[27] T. Schulz, Untersuchung Der Phasentransformationen von Hexatriacontan-Tricosan-Mischungen, Clausthal University of Technology, Clausthal-Zellerfeld, 2024. Bachelor Thesis.
[28] L. Roblès, Mise au point sur le comportement énergétique et cristallographique des n-alcanes, II Sér. C 22 (1998) 92–111.
[29] A.-J. Briard, M. Bouroukba, D. Petitjean, N. Hubert, M. Dirand, Experimental enthalpy increments from the solid phases to the liquid phase of homologous n-alkane series (C18 to C38 and C41, C44, C46, C50, C54, and C60), J. Chem. Eng. Data 48 (3) (2003) 497–513, https://doi.org/10.1021/je0201368.
[30] C.M. Earnest, J. Jones, A. Dunn, On the study of thermal transitions in selected n-paraffins using differential scanning calorimetry, Thermo 2 (3) (2022) 3, https://doi.org/10.3390/thermo2030021. Art. no.
[31] V. Jain, M.C. Biesinger, M.R. Linford, The gaussian-lorentzian sum, product, and convolution (Voigt) functions in the context of peak fitting X-ray photoelectron spectroscopy (XPS) narrow scans, Appl. Surf. Sci. 447 (2018) 548–553, https://doi.org/10.1016/j.apsusc.2018.03.190.
[32] A. Hammami, A.K. Mehrotra, Thermal behaviour of polymorphic *n*-alkanes: effect of cooling rate on the major transition temperatures, Fuel 74 (1) (1995) 96–101, https://doi.org/10.1016/0016-2361(94)P4338-3.
[33] S. Wang, K.-I. Tozaki, H. Hayashi, H. Inaba, H. Yamamoto, Observation of multiple phase transitions in some even n-alkanes using a high resolution and super-sensitive DSC, Thermochim Acta 448 (2) (2006) 73–81, https://doi.org/10.1016/j.tca.2006.06.022.
[34] L. Wang, Z.-C. Tan, S.-H. Meng, D.-B. Liang, Low-temperature heat capacity and phase transition of n-hexatriacontane, Thermochim Acta 342 (1–2) (1999) 59–65, https://doi.org/10.1016/S0040-6031(99)00308-1.
[35] R.M. Stephenson and S. Malanowski, "Handbook of the thermodynamics of organic compounds," 1987, doi: 10.1007/978-94-009-3173-2.
[36] A.A. Schaerer, C.J. Busso, A.E. Smith, L.B. Skinner, Properties of pure normal alkanes in the C_1_7 to C_3_6 range, J. Am. Chem. Soc. 77 (1955) 2017–2019.
[37] V. Piacente, D. Fontana, P. Scardala, Enthalpies of vaporization of a homologous series of n-alkanes determined from vapor pressure measurements, J. Chem. Eng. Data 39 (2) (1994) 231–237, https://doi.org/10.1021/je00014a009.
[38] E. Marti, E. Kaisersberger, W.-D. Emmerich, New aspects of thermal analysis, part I. Resolution of DSC and means for its optimization, J. Therm. Anal. Calorim. 77 (3) (2004) 905–934, https://doi.org/10.1023/B:JTAN.0000041669.06816.36.
[39] A.P. Kudchadker, B.J. Zwolinski, Vapor pressure and boiling points of normal alkanes, C _2_1 to C _1_0_0, J. Chem. Eng. Data 11 (2) (1966) 253–255, https://doi.org/10.1021/je60029a039.
[40] K. Khimeche, Y. Boumrah, M. Benziane, A. Dahmani, Solid–liquid equilibria and purity determination for binary n-alkane naphthalene systems, Thermochim Acta 444 (2) (2006) 166–172, https://doi.org/10.1016/j.tca.2006.03.011.
[41] E.S. Domalski, E.D. Hearing, Heat capacities and entropies of organic compounds in the condensed phase. Volume III, J. Phys. Chem. Ref. Data 25 (1) (1996) 1, https://doi.org/10.1063/1.555985.
[42] J.C. Company, Measurement and interpretation of crystallization equilibriums of heavy paraffin and aromatic hydrocarbon solutions, Chem. Eng. Sci. 28 (1973) 318–323.
[43] J.S. Chickos, W. Hanshaw, Vapor pressures and vaporization enthalpies of the n -alkanes from C _3_1 to C _3_8 at T = 298.15 K by correlation gas chromatography, J. Chem. Eng. Data 49 (3) (2004) 620–630, https://doi.org/10.1021/je030236t.